rPET Detectors Design and Data Processing

Juan José Vaquero, *Senior Member, IEEE,* Eduardo Lage, Lorena Ricón, Mónica Abella, Esther Vicente, Manuel Desco

***Abstract*—Small animal PET systems based on rotating planar detectors posses some interesting advantages for high sensitivity, high resolution imaging. We have designed the rPET detectors based on MLS crystals assembled on a 30 x 30 matrix optically coupled to a flat-panel PS-PMT. Weighted position readout circuits pre-process the 64 signals from the 8 x 8 anodes matrix, which are digitized using a charge-integrating converter. The amplification electronics, including the trigger ouput for coincidence detection, and the high voltage supply are integrated in a three PCBs stack that forms the base attached to the back of the PMT. The whole assembly is enclosed in a light tight, lead (Pb) shielded aluminum box. The detectors are mounted on a rotating gantry with more than 180 degrees rotation span. The digitized events are screened and histogramed, and a modified center of gravity algorithm removes from the position calculation those signals with poor signal to noise ratio. Apparent mean crystal size on the 511 keV field-flood images is 0.6 mm, mean peak-to-valley ratio is better than 8, and intrinsic resolution is 1.5 mm at the central row, with the energy window wide open. Sensitivity (CPS) for a pair of these detectors set in coincidence at 160 mm distance is 1%.**

***Index Terms*— Gamma detectors, position sensitive photomultiplier tubes, positron emission tomography (PET), small animal imaging, biomedical nuclear imaging**

I. Introduction

Small animal PET systems based on rotating planar detectors are an alternative, cost effective research tool for molecular imaging, and posses some interesting advantages for high sensitivity, high resolution imaging [1-9]. The planar detectors are usually built around compact sensors with a high accuracy in the location of the event.

These sensors must offer a high sensitivity to the gamma radiation while maintaining a high count rate capability and high random coincidence rejection. Different designs can be found in the literature using different scintillator materials, crystal sizes and coupling methods. Simultaneous high sensitivity and high spatial resolution constrains the engineering of these types of detectors since state-of-the-art technology usually confronts both requirements [10-16].

Manuscript received November 14, 2005. Part of this work is founded by the IM3 network (G03/185 Ministerio de Sanidad), with grants from the Ministerio de Educación y Ciencia, project TEC2004-07052-C02-01, and Ministerio de Industria, Turismo y Comercio project FIT-330101-2004-3. J.J. Vaquero has support from the "Ramón y Cajal" Program, Ministerio de Educación y Ciencia.

J.J. Vaquero is with the Unidad de Medicina y Cirugía Experimental, Hospital GU Gregorio Marañón, Madrid, Spain (corresponding author phone: +34-91-426-5067; fax: +34-91-426-5067; e-mail: juanjo@mce.hggm es).

E. Lage, L. Ricón, M. Abella, E. Vicente and M. Desco are with Unidad de Medicina y Cirugía Experimental, Hospital GU Gregorio Marañón, Madrid, Spain.

The detector presented in this paper was envisioned for high resolution small imaging (mice and rats mainly) looking for the maximum performance achievable at a reasonable cost since the system that will integrate these detectors should be kept simple and small.

Here we report the design and performance characteristics of this detector module, based on position sensitive photo-multipliers (PS-PMT) directly coupled to a lutetium based scintillator crystal array.

II. Materials and Methods

A. Detectors

rPET detectors are based on 1.5x1.5x12 mm^3 MLS crystals (Glendfield Partners, Canada) with all the facets mechanically polished. MLS is a not hygroscopic and rugged material based on Lutetium, what makes it radioactive, producing a background of 260 cps per cubic centimeter [13, 17]. The individual crystals are assembled on a 30 x 30 matrix with 100 microns thick Lumirror reflector (Toray Corp., Japan) between crystals, achieving a packing fraction of 88%. The array is optically coupled to an H8500 flat-panel PS-PMT (Hamamatsu, Japan) [18, 19] using silicon grease BC-630 (Bicron/SaintGobain, The Netherlands) which index of refraction is 1.465. Weighted position readout circuits pre-process the 64 signals from the 8 x 8 anodes matrix which, in turn, are amplified without shaping and digitized using a charge integrating converter (A&D Precision, MA). This readout scheme, although in its current implementation suffers from the same detector dead-time limitation described in [20], implements a modified center of gravity (COG) calculation for the event positioning [7, 21-24], and integrates gain compensation for each individual anode.

The amplification electronics, including the trigger signal for coincidence detection and the high voltage supply are contained in three stacked PCBs, forming a base attached to the back of the PS-PMT (Fig. 1). The whole assembly is enclosed in a light tight, lead (Pb) shielded aluminum box that doubles as an EM screen.

Previous works referenced in the literature [13, 16, 25] have demonstrated that this combination of PS-PMTs, high light output scintillators arrays and charge sensitive readouts schemes is well suited for high resolution, high sensitivity PET imaging systems.

B. Data acquisition and processing

The analog base output is directly connected to the charge integrating ADCs with a multi-coaxial cable, and the digitized events are screened and histogramed. A modified COG algorithm eliminates from the position calculation those anode

signals with poor signal to noise ratio. The method used to filter these signals is based on setting a dynamic threshold value, calculated for each event. If the integrated charge for any given signal is greater than the calculated threshold, it is included in the COG calculation; otherwise the anode signal is excluded. The resulting position value is mapped to an individual crystal by means of a look up table (LUT) previously computed, and the energy value for that event is histogramed on the corresponding crystal spectrum.

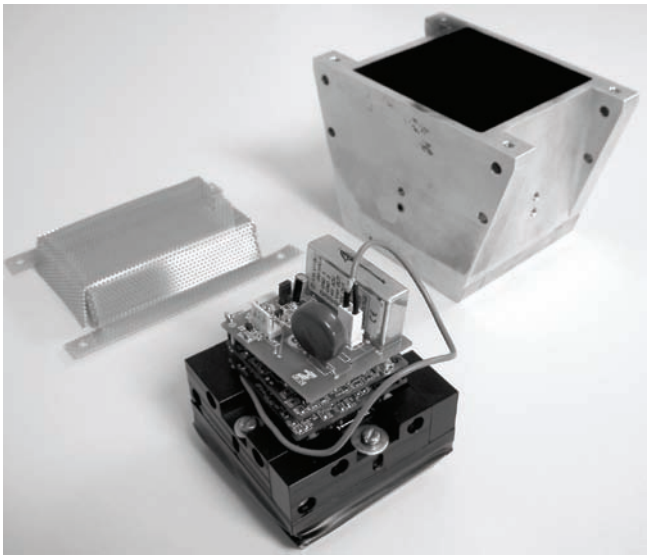

Figure 1: rPET detector: the crystal array and the PS-PMT are packed together in a black Delrim enclosure, with the detector electronics directly coupled to the PS-PMT sockets (front). This assembly fits on the aluminum Pb-shielded box (back-right) in which the detector is locked. The RF shield (back-left) closes the detector box.

The data acquisition system trigger is done using the last dynode signal from the PS-PMT, amplified at the base and filtered by a high-low discriminator that selects those events whose energy is within the hardware window energy (50 ~800 keV). This single, wide energy window is set for the whole PS-PMT, preventing the truncation of individual crystal spectra with different gains. This scheme allows compensating for gain variation across the detector field of view (FOV) by means of a variable software energy window whose variation follows the gain variation pattern.

C. *Event positioning and spatial resolution*

Homogeneous field-flood illumination and point source scans were used to characterize the ability of the detector to clearly identify the line of response (LOR) and, in turn, the crystal of interaction. The crystal LUT was obtained from a field-flood illumination image of the detector; this field-flood image is the spatial histogram of the results of the COG calculation on a 256 x 256 pixels matrix. An automatic algorithm identifies the pixel cluster that represents each crystal illumination (peak) and segments the surrounding region following a watershed approach that depicts the borders (valleys) between crystals. A final manual correction allows the user to modify segmentations errors on those regions where the algorithm does not resolve the crystals with enough accuracy.

Intrinsic resolution and spatial linearity of the detector were determined by scanning a ^{22}Na point source across its FOV on 0.3 mm steps. A twin detector was used to create a narrow photon beam by means of electronic collimation [16]; only LORs impinging perpendicularly on the crystals were accepted to create the individual crystal profiles. Apparent crystal size (FWHM) and crystal separation are computed by fitting a Gaussian to each crystal profile, and averaging the resulting parameters for the 18 crystals scanned.

D. *Gain uniformity and energy resolution*

The energy spectra calibration for each crystal was done with a field-flood illumination of the detector with two different energies: a 364 keV single photon emitter source (^{131}I) and a positron emitter source (^{18}F). For the single photon source, the tube was set in coincidence with itself and the photopeak obtained was used to calibrate the 511 keV spectra assuming a linear behavior of the detector spectral response between 80 and 750 keV, a reasonable assumption for these types of PS-PMTs [18, 19, 26, 27].

Since the gain across the detector surface is not constant, the photopeak channel energy and the spectrum scale factor for each crystal were stored in a LUT, in such a way that the energy for each event is scaled to a common reference. This procedure allows applying a single software energy window for the whole detector in real time during data acquisition. The event energy is computed by adding the values of the anode signals used for the event positioning calculation. Crystals on the edges have a worst energy resolution than the central ones due to the edge effect of the PS-PMT [28]. However since they represent a low proportion of the total, they were also used. Energy resolution measurements were done for each individual crystal and for the "average spectrum" formed by aligning and scaling each individual spectrum to a common reference, and averaging all of them. This "average energy resolution" differs from the energy resolution averaged from all the individual ones, and it better represents the detector effective energy resolution.

The individual energy scaling factors LUT is the total gain map of the detector, and represents the accumulated result of all the effects affecting the gain: crystal intrinsic quality, crystal coupling to the PS-PMT window, and PS-PMT local gain. The total gain surface was computed for each individual crystal by adding together all the spectra under the group of pixels defined by the crystal LUT. This procedure could be improved by analyzing each pixel spectrum before binning it into a crystal, and using energy and position criteria to refine the crystal LUT definition; this technique has not been applied in is this work.

III. RESULTS

The detector event positioning and spatial linearity performances have been characterized in terms of apparent crystal size and peak to valley ratio on field-flood images (Fig.

2). Profiles across central lines on 511 keV (^{18}F) field-flood image were drawn, and apparent pixel width of 0.6 mm and mean peak-to-valley ratio better than 8 were measured. The previously reported "connect-the-dot" pattern [16] was not visible in these field-flood illuminations. The right upper panel in Fig. 2 depicts the 511 keV (^{18}F) field-flood illumination and the left upper panel is the 364 keV (^{131}I) source image. Both images were created without applying any software energy window; although the 511 keV image seems very uniform, the 364 keV image shows some degradation on the upper-left and lower-right corners, which correlates very well with the gain variation map described below.

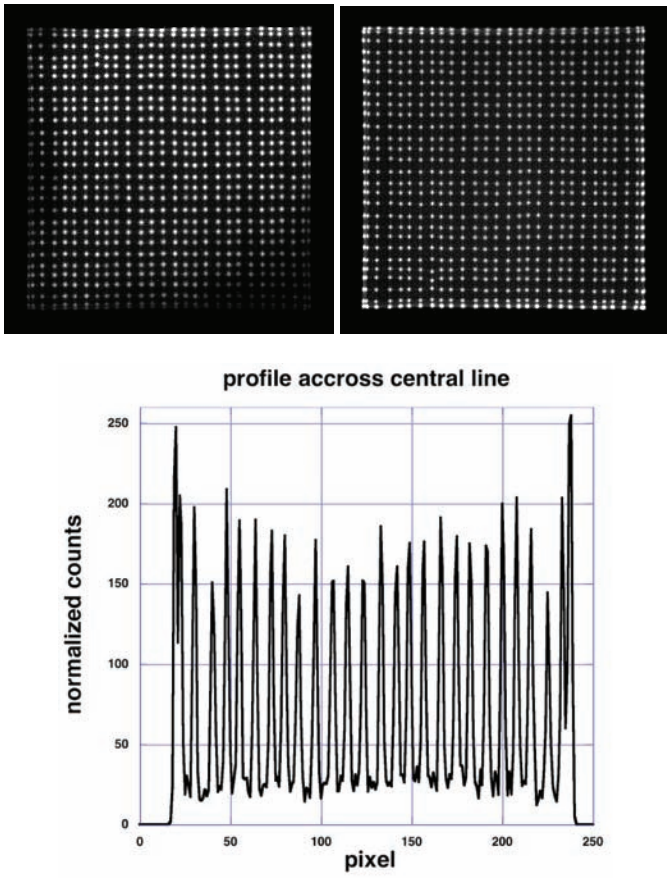

Figure 2: Detector imaging performance: 364 keV (^{131}I) field-flood (upper left); 511 keV (^{18}F) field-flood image (upper right). Profile across central line of the 511 keV image (normalized to 255). Apparent pixel width is 0.6 mm and mean peak-to-valley ratio is 8.

The average intrinsic resolution of the 18 crystals scanned profiles is 1.5 mm, that equals to the actual crystal size. The average peak separation is 1.6 mm (Fig. 3), matching the crystal pitch. The height of those peaks varies following the gain surface profile depicted in Fig. 4.

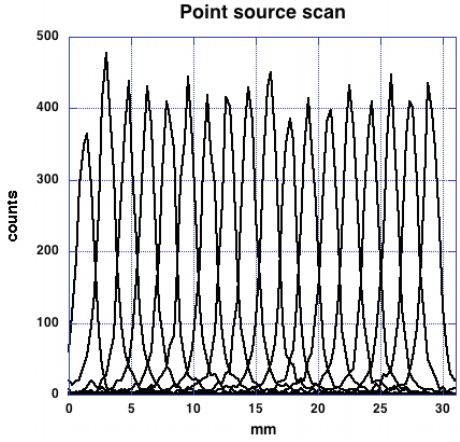

Figure 3: Detector module spatial resolution for 18 crystals at the central line; an electronically collimated ^{22}Na point source was scanned across the central line of the array at 0.3 mm steps. The average FWHM of the crystal profiles is 1.5 mm and the average peak separation is 1.6 mm.

The photopeak channel for each crystal is a measurement of the gain uniformity across the tube surface. Left panel in Fig. 4 depicts the total gain variation. This parameter depends not only on the intrinsic properties of the crystal and the photomultiplier area under it, but also on the quality of the coupling between them. The right panel in Fig. 4 represents the component of the gain surface variation due exclusively to the different anode gains; since the number of the resolved crystals (784) is higher than the number of anodes (64), the total gain variation surface is more densely sampled and consequently shows more texture than the anode gain surface, but there is a direct correlation between both surfaces.

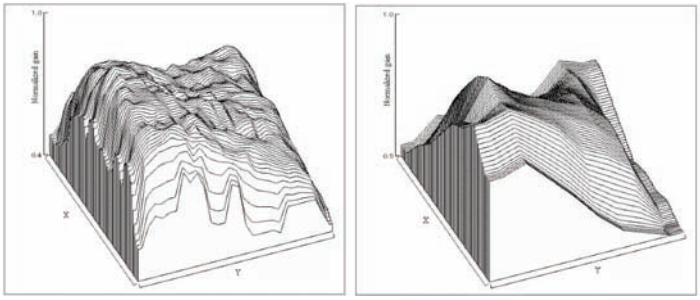

Figure 4: Normalized gain uniformity. Left: gain computed from the energy spectra for each crystal and adjusting the 511 keV photopeak. Right: anode gain measured at the factory by the PS-PMT manufacturer. Both surfaces follow the same general pattern. The finer textured appearance of the energy gain (left) is due to variations on the individual crystal and optical coupling characteristics and are more relevant on the edges.

The single photon 364 keV photopeak from the ^{131}I source was used for calibration to accurately quantify the detector energy resolution. Count-rate due lutetium background in the single photon acquisitions was negligible compared with the ^{131}I photon count-rate. The mean energy resolution across the tube surface, excluding the outlier crystals on the edges, was 16.5 % with a standard deviation of 2. The worst crystal energy resolution in this detector was 23.4 %, while the best one was 12.7 %. Fig. 5 shows on the left, the energy spectrum

for one of the central crystals in which the energy resolution is 13.5 %, and on the right the averaged spectrum for the whole tube after all the photpeaks were scaled and aligned; the energy resolution measured on this averaged spectrum is 19.6 %.

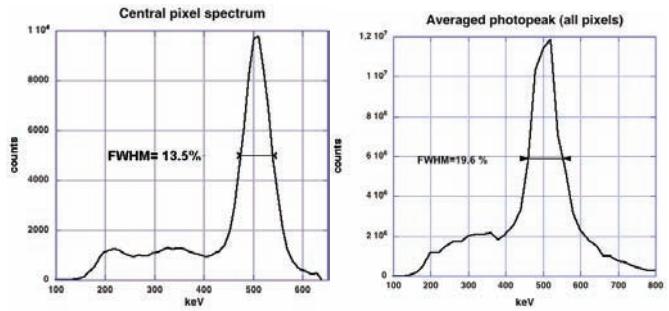

Figure 5: Left: energy spectrum for one of the central crystals. Right: averaged energy spectrum for the detector after all the individual crystals were scaled and aligned to a common reference channel.

IV. DISCUSSION

Individual crystal can be clearly identified in Fig 2, although the PS-PMT useful FOV can only resolve a matrix of 28 x 28 crystals from the original 30 x 30. The position performace of this detector provides a good spatial sampling due to the high peak to valley ratio. The connect-the-dot pattern previously reported is not visible on this detector because the valley width and its ground level make it very difficult to appreciate. It is also well known that a good event positioning is not enough since this information by itself cannot distinguish between scatter and photoelectric absorption. To resolve this, a good energy resolution is required. Fig. 5 depicts an individual crystal spectrum in which energy resolution is good enough to satisfy this requirement. If energy windowing is aplied individually to each crystal, it is reasonable to expect a good global performance of the detector in terms of scatter rejection. This could be further improved if each pixel spectrum were analyzed before binning it into a crystal spectrum, using not only the position criteria but also the energy criteria to refine the crystal LUT definition.

Gain uniformity across the detector surface is dominated by the individual anode gain variation of the PS-PMT. Our PS-PMT readout circuit allows for an individual anode compensation, still not activated in these initial tests. These results show that if the individual gain adjust techniques really compensate this gain variation, a better energy resolution uniformity could be achieved.

V. CONCLUSIONS

We have demonstrated that detector modules created by coupling this large area PS-PMTs and compact arrays of small individual crystals can locate the end point of a line of response of a positron annihilation event with the accuracy required for high resolution small animal PET scanners. Designs that use direct coupling of the scintillators to the new flat panels PS-PMTs can achieve a larger packing fraction compared with the small metal PS-PMTs, since the active surface to dead area around the tube ratio is much higher with these new devices. However, the active surface to dead time ratio is lower, since conventional readout schemes will not distinguish or reject simultaneous events occurring on different the large area flat panel. Until the new readout strategy is fully implemented, maximum singles count rate for these types of detector will be limited by the pile-up effect occurring when two or more gamma photons coming from different events hit simultaneously the detector active surface.

The proposed detector and its signal processing described in this work have proved to be useful for in high resolution small animal PET systems. Future research will focus on the detector dead time issue since having a larger active detector area increases the rate of in-detector piled-up events for high count rates. Processing the anodes in parallel has been proposed [20] as an interesting alternative.

ACKNOWLEDGMENT

The authors thank SUINSA Medical Systems Engineering Department for their support with the detector design and manufacturing.

REFERENCES

[1] S. R. Cherry, "Recent Advances in Instrumentation for Positron Emission Tomography," *Nuclear Instruments & Methods in Physics Research*, vol. 348, pp. 577-582, 1994.

[2] P. D. Cutler, S. R. Cherry, E. J. Hoffman, W. M. Digby, and M. E. Phelps, "Design Features and Performance of a PET System for Animal Research," *Journal of Nuclear Medicine*, vol. 33, pp. 595-604, 1992.

[3] F. De Notaristefani, R. Pani, F. Scopinaro, L. M. Barone, K. Blazek, G. De Vincentis, T. Malatesta, P. Maly, R. Pellegrini, A. Pergola, A. Soluri, and F. Vittori, "First Results from a YAP:Ce Gamma Camera for Small Animal Studies," *IEEE Transaction on Nuclear Science*, vol. 43, pp. 3264-3271, 1996.

[4] R. Lecomte, J. Cadorette, P. Richard, S. Rodrigue, and D. Rouleau, "Design and Engineering Aspects of a High-Resolution Positron Tomograph for Small Animal Imaging," *IEEE Transactions on Nuclear Science*, vol. 41, pp. 1446-1452, 1994.

[5] S. Siegel, S. R. Cherry, A. R. Ricci, Y. P. Shao, and M. E. Phelps, "Development of Continuous Detectors for a High-Resolution Animal PET System," *IEEE Transactions on Nuclear Science*, vol. 42, pp. 1069-1074, 1995.

[6] M. Watanabe, H. Uchida, H. Okada, K. Shimizu, N. Satoh, E. Yoshikawa, T. Ohmura, T. Yamashita, and E. Tanaka, "A High Resolution PET for Animal Studies," *IEEE Transactions on Medical Imaging*, vol. 11, pp. 577-580, 1992.

[7] R. Pani, R. Pellegrini, M. N. Cinti, C. Trotta, G. Trotta, F. Garibaldi, R. Scafe, and A. Del Guerra, "Flat Panel PMT for Photon Emission Imaging," *Nuclear Instruments & Methods in Physics Reseach Section A*, vol. 505, pp. 590-594, 2003.

[8] J. S. Huber and W. W. Moses, "Conceptual design of a high-sensitivity small animal PET camera with 4π coverage," *Nuclear Science, IEEE Transactions on*, vol. 46, pp. 498-502, 1999.

[9] N. Zhang, C. J. Thompson, C. L. Thompson, and K. Q. Nguyen, "Improving the performance of small planar detectors for dedicated PET instruments," *Nuclear Science, IEEE Transactions on*, vol. 49, pp. 111-115, 2002.

[10] S. R. Cherry, Y. Shao, R. W. Silverman, K. Meadors, S. Siegel, A. Chatziioannou, J. W. Young, W. F. Jones, J. C. Moyers, D. Newport, A. Boutefnouchet, T. H. Farquhar, M. Andreaco, M. J. Paulus, D. M. Binkley, R. Nutt, and M. E. Phelps, "MicroPET - a High-Resolution PET Scanner for Imaging Small Animals," *IEEE Transactions on Nuclear Science*, vol. 44, pp. 1161-1166, 1997.

[11] F. Daghighian, D. M. Lovelock, B. Eshaghian, P. Shenderov, J. D. Willins, C. L. Melcher, J. S. Schweitzer, R. A. Manente, and C. A. Peterson, "Design Considerations of an Animal PET Scanner Utilizing LSO Scintillators and Position Sensitive PMTs," presented at Nuclear Science Symposium & Medical Imaging Conference, Norfolk, Virginia, USA, 1995.

[12] S. E. Derenzo, W. W. Moses, H. R. H., and T. F. Budinger, "Critical Instrumentation issues for <2mm resolution, high sensitivity brain PET," in *Quantification of Brain Function*, N. A. L. K. Uemura, T. Jones, et al., Ed. Amsterdam: Elsevier Science Publishers, 1993, pp. 25-37.

[13] R. S. Miyaoka, S. G. Kohlmyer, J. Joung, and T. K. Lewllen, "Performance Characteristics of a Second Generation Micro Crystal Element (MiCE2) Detector," *2001 IEEE Nuclear Science Symposium Conference Record*, vol. 2, pp. 1124-1127, 2001.

[14] J. Seidel, W. R. Gandler, and M. V. Green, "Characteristics of a Pair of Small-Field-of-View LSO Scintillation Cameras," *IEEE Transactions on Nuclear Science*, vol. 43, pp. 1968-1973, 1996.

[15] J. Seidel, J. J. Vaquero, S. Siegel, W. R. Gandler, and M. V. Green, "Depth Identification Accuracy of a Three-Layer Phoswich PET Detector Module," *IEEE Trans Nucl Sci*, vol. 46, pp. 485-490, 1999.

[16] J. J. Vaquero, J. Seidel, S. Siegel, W. R. Gandler, and M. V. Green, "Performance Characteristics of a Compact Position-Sensitive LSO Detector Module," *IEEE Trans Med Imag*, vol. 17, pp. 967-978, 1998.

[17] C. L. Melcher and J. S. Schweitzer, "Cerium-doped Lutetium Oxyorthoslicate: A Fast, Efficient New Scintillator," *IEEE Transaction on Nuclear Science*, vol. 39, pp. 502-505, 1992.

[18] R. Engels, U. Clemens, G. Kemmerling, and J. Schelten, "High spatial resolution scintillation detector based on the H8500 photomultiplier," *2003 IEEE Nuclear Science Symposium Conference Record*, vol. 1, pp. 692 - 695, 2003.

[19] N. Inadama, H. Murayama, M. Watanabe, T. Omura, T. Yamashita, H. Kawai, T. Umehara, T. Kasahara, N. Orita, and T. Tsuda, "Performance of a PET detector with a 256ch Flat Panel PS-PMT," *IEEE Transactions on Nuclear Science*, vol. 51, pp. 58-62, 2004.

[20] S. Riboldi, J. Seidel, M. Green, J. Monaldo, J. Kakareka, and T. Pohida, "Investigation of signal readout methods for the Hamamatsu R8500 flat panel PSPMT," *2003 IEEE Nuclear Science Symposium Conference Record*, vol. 4, pp. 2452 - 2456, 2003.

[21] P. D. Olcott, J. A. Talcott, C. S. Levin, F. Habte, and A. M. K. Foudray, "Compact Readout Electronics for Position Sensitive Photomultiplier Tubes," *2003 IEEE Nuclear Science Symposium Conference Record*, vol. 3, pp. 1962-1966, 2003.

[22] V. Popov, S. Majewski, and A. G. Weisenberger, "Readout Electronics for Multianode Photomultiplier Tubes With Pad Matrix Anode Layout," *2003 IEEE Nuclear Science Symposium Conference Record*, vol. 3, pp. 2156 - 2159, 2003.

[23] V. Popov, S. Majewski, A. G. Weisenberger, and R. Wojcik, "Analog Readout System with Charge Division Type Output," *2001 IEEE Nuclear Science Symposium Conference Record*, vol. 4, pp. 1937-1940, 2001.

[24] S. Siegel, R. W. Silverman, Y. Shao, and S. R. Cherry, "Simple Charge Division Readouts for Imaging Scintillator Arrays Using a Multi-Channel PMT," *IEEE Trans Nucl Sci*, vol. 43, pp. 1634-1641, 1996.

[25] S. Majewski, D. Kieper, E. Curran, C. Keppel, B. Kross, A. Palumbo, V. Popov, A. G. Weisenberger, B. L. Welch, R. Wojcik, M. B. Williams, A. R. Goode, M. More, and G. Zhang, "Optimization of Dedicated Scintimammography Procedure Using Detector Prototypes and Compressible Phantoms," *IEEE Transactions on Nuclear Science*, vol. 48, pp. 822-829, 2001.

[26] K. K. Hamamatsu-Photonics, "Position Sensitive Photomultiplier Tube R5900-00-C8 and R5900U-00-C8," in *Data Sheet*. Japan, 1996.

[27] K. K. Hamamatsu-Photonics, "Flat-Panel Type Multianode Photomultiplier Tube Assembly H8500." Japan, 2003.

[28] R. L. Clancy, C. J. Thompson, J. L. Robar, and A. M. Bergman, "A Simple Technique to Increase the Linearity and Field-of-View in Position Sensitive Photomultiplier Tubes," *IEEE Transactions on Nuclear Science*, vol. 44, pp. 494-498, 1997.